Original Paper

Charge effects on quinoline hydrodenitrogenation catalyzed by Ni−Mo−S active sites-A theoretical study by DFT calculation

Si-Jia Ding [a], Shao-Zhong Peng [a], Zuo-Jie Yan [b], Ji-Feng Wang [a], Shu-Jiao Jiang [a], Zhan-Lin Yang [a, *]

[a] Dalian Research Institute of Petroleum and Petrochemicals, SINOPEC, Dalian, 116041, China
[b] Fushun Petrochemical Company, Fushun, Liaoning, 113001, China

ARTICLE INFO

ABSTRACT

The charge distribution on Ni−Mo−S active sites can affect hydrodenitrogenation (HDN) activity. In this study, a series of model Ni−Mo−S were developed with various charge distributions. For comparison, the charge distribution effects on quinoline HDN were studied. The results show that a lack of electrons and extra protons can both lower the orbital eigenvalue of the Ni−Mo−S, leading to stronger adsorption of nitrogen-containing compounds and inhibition of ammonia desorption. Electron deficiency will improve the generation of active hydrogen on the active sites but inhibit hydrogen transfer to the nitrogen compounds; extra protons can provide H^+ to the nitrogen compounds, which will flexibly transfer between the nitrogen compound and active sites, thus improving the cleavage of the C−N bond.
© 2021 The Authors. Publishing services by Elsevier B.V. on behalf of KeAi Communications Co. Ltd. This is an open access article under the CC BY-NC-ND license (http://creativecommons.org/licenses/by-nc-nd/4.0/).

1. Introduction

With the adjusted energy structure and change in the supply-demand relationship, the production capacity of fossil fuels in the petrochemical industry is decreasing gradually, while the production capacity of chemical raw materials must be urgently strengthened. Hydrocracking technology is an important process for the petrochemical industry to convert distillates into chemical raw materials (Bezergianni et al., 2009; Choudhary and Saraf, 1975; Köseoḡ;lu and Phillips, 1987; Scherzer Jg, 1996). In general, hydrocracking catalysts contain acidic zeolites as the cracking center (Ali et al., 2002; Martens et al., 2001; Speight, 2020; Zhang et al., 2007), and the nitrogen contents, particularly the basic nitrogen compounds in the cracking feedstock, are strictly limited. To remove the nitrogen compounds in the feedstock, a hydrocracking pretreatment catalyst is required in the hydrocracking process (Badoga et al., 2020; Kohli et al., 2019; Oh et al., 2019; Prada Silvy et al., 2019).

The prevailing commercial pretreatment catalysts are highly active Mo−Ni bimetal γ-alumina-supported hydrotreating catalysts.

Strong acidic supports and electronegative elements can significantly improve the removal of nitrogen compounds (Hu et al., 2019; Tung et al., 2017; Valles et al., 2019; Yao et al., 2017; Tang et al., 2017). These prompters could cause electron deficiency or bring extra protons to the Ni−Mo−S active nanoclusters via inductive effects or charge transfer (Prins et al., 1997; Tominaga and Nagai, 2010). With the rapid development of computer technology and the progress of quantum chemical calculations, theoretical calculations of complex catalytic processes, such as charge distribution effects on hydrodenitrogenation, can be implemented.

In this study, quinoline, which is a typical basic two-ring nitrogen compound for hydrodenitrogenation (HDN) research (Li et al., 2012; Lu et al., 2007), is used as the probe, and a series of model Ni−Mo−S with different charge distributions are used as the active sites. The key processes of quinoline HDN, including adsorption, hydrogenation saturation, and C−N bond cleavage on the Ni−Mo−S, are calculated by quantum chemistry calculations.

2. Modeling and computational methods

The neutral Ni−Mo−S model in this study was a hexagonal single-layer nanocluster. The stable state of the Ni−Mo−S active sites under the hydrogenation reaction is shown in Fig. 1 (Ding et al., 2018a). Previous studies have shown that on the Ni(Co)−

---

* Corresponding author.
E-mail address: yangzhanlin.fshy@sinopec.com (Z.-L. Yang).

List of symbols

E_{ad}	Adsorption energy
L_b	Bond length
O_m	Mayer bond order
E_r	Reaction Energy
E_a	Activation Energy

Table 1
Atomic dispersion parameters.

Element	H	C	N	S	Ni	Mo
R_0	1.001	1.452	1.397	1.683	1.562	1.639
C_6	1.451	18.134	12.748	57.729	111.943	255.686

Mo—S or MoS_2, the hydrogenolysis active centers are mainly located on the (10-10) plane, denoted as the Ni(Co)—Mo edge (Ding et al., 2017a, 2017b, 2018a,b; Sun et al., 2004; Sylvain et al., 2004). In this study, the issues of quinoline HDN are focused on the Ni—Mo edge of the Ni—Mo—S active sites. Considering the symmetry of the calculation model, in the electron deficiency case, three pairs of electrons were subtracted from the Ni—Mo—S, and the model is denoted as E-Ni-Mo-S. For additional protons, one proton was added to each Ni—Mo edge, and the model was denoted as P—Ni—Mo—S.

Calculations were performed using the DMol3 code. The calculation function is the general gradient approximation-Perdew-Burke-Ernzerhof function, and the basis set is a double numerical plus polarization basis (Chigo Anota and Cocoletzi, 2014; Delley and B. 1982). To analyze the transition state, the open shell mode was used to treat the electron spin. The symmetry in the calculation was also canceled to meet the anisotropy in the HDN process. The orbital cut off is unified to 5.0 Å for every atom. To balance the calculation speed and accuracy, the effective core potential (ECP) method was used to simplify the core electron treatment, and thermal smearing was set to 5×10^{-4} Hartree. The self-consistent field density convergence (SCF) was set to 2×10^{-5}, and the energy tolerance for the geometry optimization and transition state was 2×10^{-5} Hartree. The force tolerance was 4×10^{-3} Ha/Å geometry optimization and 3×10^{-3} Ha/Å for the transition search. The Grimme 06 correction method was used to calculate the atomic dispersion. The exchange-correlation dependent factor s_6 was set to 1.0, and the damping coefficient was set to 20.0. The dispersion parameters for the atoms involved in this calculation can be found in Table 1 (Grimme, 2010, 2011).

During the process of HDN, the adsorption of reactants on the active sites relies on the interactions between the lone or conjugated electron pairs of the reactants and the unoccupied molecular orbitals of the active sites. According to acid-base theory, E-Ni-Mo-S can protonate basic nitrogen compounds. The changes in molecular orbitals before and after the protonation of quinoline (Q), tetrahydroquinoline (THQ), and decahydroquinoline (DHQ) (THQ and DHQ are important intermediates in the hydrodenitrogenation process of quinoline (Luan et al., 2009) and are shown in Table 2. The highest occupied molecular orbital (HOMO) of nonprotonated basic nitrogen compounds is mainly contributed by the lone pair electrons on the nitrogen atoms. When the nitrides are protonated by E-Ni-Mo-S, the lone pair electrons of atoms combine with H^+. The newly generated HOMO has barely related to the nitrogen atoms, and the orbital eigenvalue is significantly reduced. This change will weaken the binding ability between the active center and the nitrogen compounds.

The effects of charge distributions on the lowest unoccupied molecular orbital (LUMO) are shown in Table 3. On the neutral Ni—Mo edge, the LUMO is attributed to the d orbital of the tetra-coordinated Ni atom and the pentacoordinated Mo atom with S atoms. The LUMO eigenvalue is −4.53 eV. On the E-Ni-Mo-S, the composition and morphology of the LUMO orbitals do not change much, and they still consist of unoccupied d orbitals from aligned metal atoms. However, the LUMO eigenvalue significantly decreases to −8.20 eV. On the P—Ni—Mo edge, the H^+ bonds are stably coordinated with the pentacoordinated Mo atom, which is near the exposed Ni atom. This combination will satisfy the stable hexacoordination of the Mo atom. The Ni atom close to H^+ will be more electron deficient, leading to a reduction in the LUMO eigenvalue. It could be concluded that both the lack of electrons and the extra protons will lower the LUMO eigenvalue and enhance the ability of receiving electrons from the reactants.
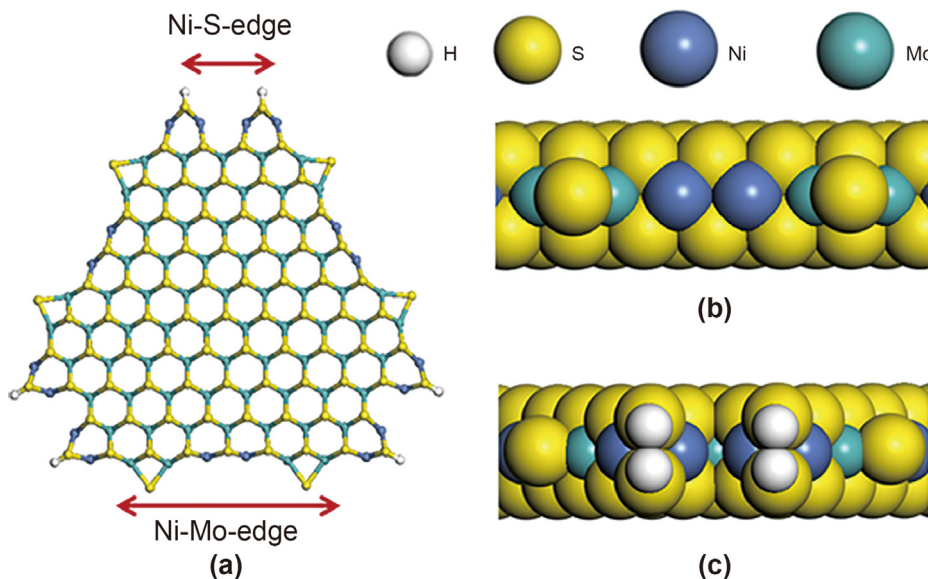

Fig. 1. Ni—Mo—S nanocluster model (a) front view of the nanocluster, (b) lateral view of the (10-10) plane and (c) lateral view of the (−1010) plane.

Table 2
Effects of H⁺ on the HOMO of Q, DHQ and THQ.

Nitrogen compounds	Q	Q-H⁺	DHQ	DHQ-H⁺	DHQ	DHQ-H⁺
HOMO						
Eigenvalues/eV	−5.73	−7.65	−4.37	−9.85	−4.90	−10.90

Table 3
Effects of charge distribution on the LUMO.

Active sites	LUMO morphology	Eigenvalue/eV
Ni−Mo−S		−4.53
E-Ni-Mo-S		−8.20
P−Ni−Mo−S		−6.31

2.1. Effects of charge distribution on the adsorption of nitrogen compounds

During the HDN process, the reactant, some important intermediates and the ammonia have strong adsorption ability on the active centers. The calculation results of the adsorption of Q, THQ, DHQ and NH₃ on Ni−Mo-edge affected by different charge distributions are shown in Table 4. On the neutral Ni−Mo−S, the formation of the nitrogen compounds adsorption is point to point. Specifically, the nitrogen atom of Q, THQ and DHQ bonded with nickel atom, forming an N−Ni bond with 2.2−2.3 Å and 0.3−0.4 Mayer bond order. The nitrogen atom of NH₃ prefers to bond with Mo atoms. The bond direction is in accord with the orientation of the LUMO morphology listed in Table 2. Because of the similarity of LUMO morphology, the adsorption morphology of the nitrogen compounds on the E-Ni-Mo-S and Ni−Mo−S active sites are similar as well, whereas the significant difference is the adsorption energy. The adsorption energies of nitrogen compounds on E-Ni-Mo-S are approximately 20−30 larger than those on the neutral Ni−Mo−S. When the nitrogen compounds adsorb on the P−Ni−Mo−S active sites, the H⁺ will transfer to the nitrogen, combing with the long pair electrons. The adsorption of nitrogen compounds will turn to flat model without forming the N−Ni bond. Despite the lacking of the single strong chemisorption bonds, the weak interaction between the conjugate π-electrons and the unoccupied orbitals the extra dispersion force from the increasing contact area both enlarge the adsorption energy. According to the calculation results, both the electron deficiency and the extra proton will enhance the adsorption of nitrogen compounds on the Ni−Mo-edge, whereas the ammonia desorption is inhibited which is negative to the recovery of the active center during the HDN process.

2.2. Effects of charge distributions on the hydrogen activation and transfer

On the Ni−Mo edge, hydrogen activation is carried out by H₂ molecule dissociation on the metal or sulfur atom. Hydrogen dissociation with adsorption of a quinoline molecule was calculated, and the results are shown in Table 5. On the Ni−Mo edge of neutral Ni−Mo−S, hydrogen dissociation is a strong endothermic step with a high energy barrier. At the corresponding position of E-Ni-Mo-S, this dissociation is an obvious exothermic process, and the activation energy significantly decreases to 108.51 kJ/mol. On the P−Ni−Mo−S, the thermal effects and activation energy charge were less significant than those on E-Ni-Mo-S. It could be predicted that electron deficiency will promote hydrogen dissociation.

The newly generated active hydrogen must transfer to the nitrogen compounds quickly in the case of self-combination. Among the several hydrogen transfers of quinoline HDN, the conversion from THQ to penta-hydroquinoline (PHQ) is a key speed control step (Ding et al., 2017; Jian and Prins, 1998). This elementary reaction on the Ni−Mo edge with different charge distributions is shown in Table 6. The active hydrogen breaks the conjugated aromatic rings. The reaction energy is up to 40−70 kJ/mol, and the activation energy exceeds 100 kJ/mol. In comparison, hydrogen transfer on neutral Ni−Mo−S is relatively easier and most difficult on E-Ni-Mo-S. The difficulty of hydrogen transfer is adverse to hydrogen dissociation, indicating that the stronger the interaction between the hydrogen and active sites, the easier the hydrogen dissociation and the harder the hydrogen transfer.

2.3. Effects of charge distributions on the C−N cleavage of nitrogen compounds

For quinoline, the main pathway of C−N bond cleavage is the E₂ elimination of DHQ. This process contains two elementary steps: the first step is hydrogen elimination of β-C, forming nona-hydroquinoline, and the second step is cleavage of the C−N bond, forming a C═C bond and amino group (Li et al., 2012). Table 7 shows the elimination of the β-H of DHQ on Ni−Mo-edges with different acid types. According to the calculated results, the transfer of β-H to the active sites is an endothermic process with high activation energy. During this step, the S accepts the hydrogen atom, and the β-C atom bonds with the Mo atom. The influence of the charge distribution is limited, whereas the H⁺ provided by B−Ni−Mo−S returns to the active sites, and the reaction energy and activation energy both decrease. The C−N bond cleavage of NHQ is shown in Table 8. The results show that the C−N break on the neutral Ni−Mo−S is a strong endothermic step with very high energy barrier. Meanwhile, the C−N bond cleaves the newly generated C═C bonds attached with the Mo atom. The electron deficiency on Ni−Mo−S does not change the pathway of C−N bond cleavage, and the influence is quite limited. Attributable to the

Table 4
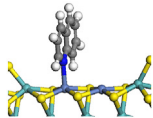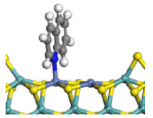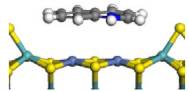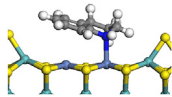Adsorption of Q, THQ and DHQ on the Ni–Mo-edge with different charge distributions.
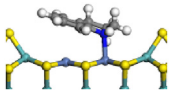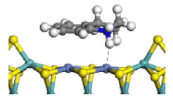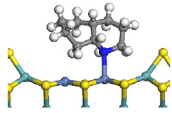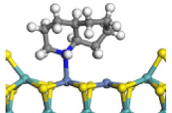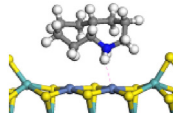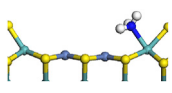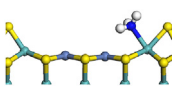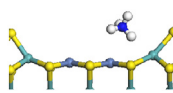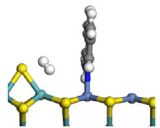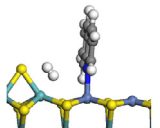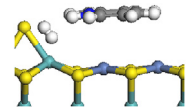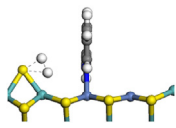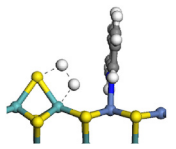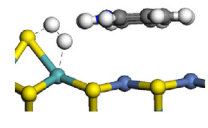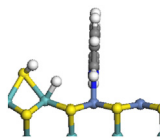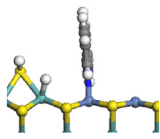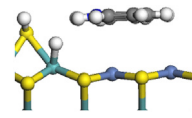
Active sites	Ni–Mo–S	E-Ni-Mo-S	P–Ni–Mo–S
Nitrogen compounds	Q		
Morphology			
E_{ad}, kJ/mol^{-1}	−97.43	−129.27	−122.32
Ni−N L_b/Å	2.2	2.1	−
Ni−N O_m	0.39	0.44	−
Nitrogen compounds	THQ		
Morphology			
E_{ad}, kJ/mol^{-1}	−106.28	−133.74	−143.36
Ni−N L_b/Å	2.2	2.2	−
Ni−N O_m	0.30	0.31	−
Nitrogen compounds	DHQ		
Morphology			
E_{ad}, kJ/mol^{-1}	−101.70	−130.84	−137.05
Ni−N L_b/Å	2.3	2.2	−
Ni−N O_m	0.35	0.33	−
NH$_3$			
Morphology			
E_{ad}, kJ/mol^{-1}	−109.71	−128.98	−124.87
Ni−N L_b/Å	2.5	2.4	−
Ni−N O_m	0.52	0.56	−

Table 5
Hydrogen dissociation with adsorbing quinoline.

Active sites	Ni–Mo–S	E-Ni-Mo-S	P–Ni–Mo–S
Reactant			
Transition state			
Product			
E_r, kJ/mol	+5.02	−17.54	−8.36
E_a, kJ/mol	+139.40	+108.51	+116.17

stronger adsorption ability of the LUMO, the energy barrier decreased by approximately 10 kJ/mol on the E-Mo-Ni-S. Notably, on the P–Ni–Mo–S, the proton transferred to the Ni–Mo-edge in the elimination step returns back to nitrogen compounds during C–N bond cleavage. The proton not only lowers the electron density but also increases the coordination of the N atom, leading to a more stable transition state of C–N bond cleavage. The activation energy decreased by approximately 40 kJ/mol, indicating that

Table 6
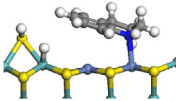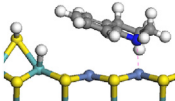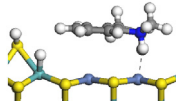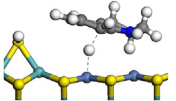Hydrogen transfer from THQ to PHQ on Ni—Mo-edge with charge distributions.
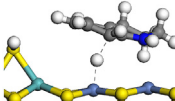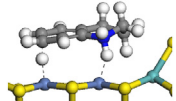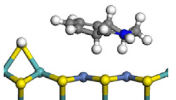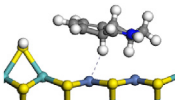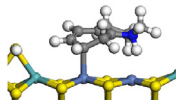
Active sites	Ni—Mo—S	E-Ni-Mo-S	P—Ni—Mo—S
Reactant			
Transition state			
Product			
E_r, kJ/mol	+48.61	+65.20	+54.34
E_a, kJ/mol	+104.25	+131.28	+123.69

Table 7
Hydrogen elimination of DHQ β-C.
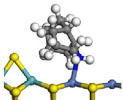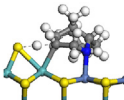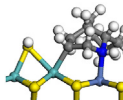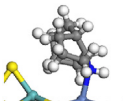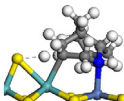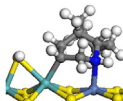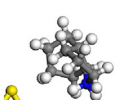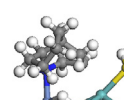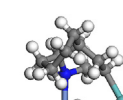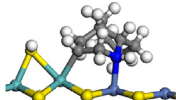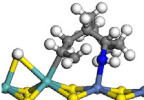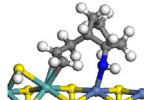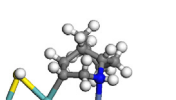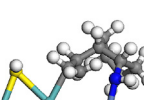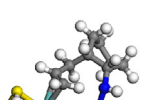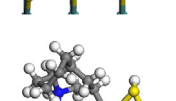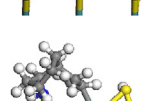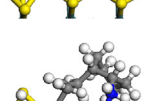
Active sites	DHQ	Transition state	NHQ	E_r, kJ/mol	E_a, kJ/mol
Ni—Mo—S				+82.32	+135.88
E-Ni-Mo-S				+80.94	+130.87
P—Ni—Mo—S				+69.84	+119.06

Table 8
C—N bond cleavage of NHQ.

Active sites	NHQ	Transition state	C—N bond break	E_r, kJ/mol	E_a, kJ/mol
Ni—Mo—S				+147.61	+187.31
E-Ni-Mo-S				+138.28	+176.05
P—Ni—Mo—S				+85.09	+145.56

flexible H$^+$ transfer between the nitrogen compounds and the active center significantly lowered the C–N bond cleavage in the HDN of quinoline.

3. Conclusions

In this study, the HDN catalytic activities of Ni–Mo–S with different charge distributions are calculated. The conclusions are as follows:

1. Electron deficiency and extra protons could both lower the LUMO eigenvalue of Ni–Mo–S. The effects of electron deficiency on the morphology are limited, whereas extra protons could change the local morphology of LUMO.
2. Electron deficiency and extra protons could both enhance the adsorption ability of Ni–Mo–S active sties to nitrogen compounds. On neutral Ni–Mo–S and E-Ni-Mo-S, the nitrogen compounds adsorb via the chemisorption N–Ni bond, whereas on P–Ni–Mo–S, the nitrogen compounds take flat adsorption. However, ammonia desorption is inhibited by electron deficiency and extra protons during the HDN process.
3. Electron deficiency on N–Mo–S promotes the generation of active hydrogen but restricts hydrogen transfer to nitrogen compounds.
4. During C–N bond cleavage, the proton of P–Ni–Mo–S can flexibly transfer between the nitrogen compounds and the active sites. In this way, the cleavage of C–N is significantly promoted.

Acknowledgments

References

Ali, M.A., Tatsumi, T., Masuda, T., 2002. Development of heavy oil hydrocracking catalysts using amorphous silica-alumina and zeolites as catalyst supports. Appl. Catal., A 233 (1), 77–90. https://doi.org/10.1016/S0926-860X(02)00121-7.

Badoga, S., Alvarez-Majmutov, A., Xing, T., et al., 2020. Co-processing of hydrothermal liquefaction biocrude with vacuum gas oil through hydrotreating and hydrocracking to produce low-carbon fuels. Energy Fuels 34 (6), 7160–7169.

Bezergianni, S., Voutetakis, S., Kalogianni, A., 2009. Catalytic hydrocracking of fresh and used cooking oil. Ind. Eng. Chem. Res. 48 (18), 8402–8406. https://doi.org/10.1021/ie900445m.

Chigo Anota, E., Cocoletzi, G.H., 2014. GGA-based analysis of the metformin adsorption on BN nanotubes. Phys. E Low-dimens. Syst. Nanostruct. 56, 134–140. https://doi.org/10.1016/j.physe.2013.08.033.

Choudhary, N., Saraf, D.N., 1975. Hydrocracking: a review. Ind. Eng. Chem. Prod. Res. Dev. 14 (2), 74–83. https://doi.org/10.1021/i360054a002.

Delley, B., 1982. Efficient and accurate expansion methods for molecules in local density models. J. Chem. Phys. 76 (4), 1949–1960. https://doi.org/10.1063/1.443168.

Ding, S., Jiang, S., Zhou, Y., et al., 2017a. Oxygen effects on the structure and hydrogenation activity of the MoS2 active site: a mechanism study by DFT calculation. Fuel 194 (APR.15), 63–74. https://doi.org/10.1016/j.fuel.2016.12.071.

Ding, S., Li, A., Jiang, S., et al., 2018a. Niobium modification effects on hydrodesulfurization of 4,6-DMDBT catalyzed on Ni-Mo-S active sites: a combination of experiments and theoretical study. Fuel. https://doi.org/10.1016/j.fuel.2018.10.002.

Ding, S., Zhou, Y., Wei, Q., et al., 2017b. Substituent effects of 4,6-DMDBT on direct hydrodesulfurization routes catalyzed by Ni-Mo-S active nanocluster-A theoretical study. Catal. Today, S092058611730737X.

Ding, S., Zhou, Y., Wei, Q., et al., 2018b. Substituent effects of 4,6-DMDBT on direct hydrodesulfurization routes catalyzed by Ni-Mo-S active nanocluster-A theoretical study. Catal. Today 305, 28–39. https://doi.org/10.1016/j.cattod.2017.10.040.

Grimme, S., 2010. Semiempirical GGA-type density functional constructed with a long-range dispersion correction. J. Comput. Chem. 27 (15), 1787–1799. https://doi.org/10.1002/jcc.20495.

Grimme, S., 2011. Density functional theory with London dispersion corrections. Wiley Interdiscipl. Rev. Comput. Mol. Sci. 1 (2), 211–228. https://doi.org/10.1002/wcms.30.

Hu, E., Yao, Z., Zhao, L., et al., 2019. Characteristics of zeolite-modified NiMo/Al2O3 catalysts and their hydrotreating performance for light cycled oil. Can. J. Chem. Eng. 97. https://doi.org/10.1002/cjce.23352.

Jian, M., Prins, R., 1998. Mechanism of the hydrodenitrogenation of quinoline over NiMo(P)/Al2O3 catalysts. Stud. Surf. Sci. Catal. 101 (1), 87–96. https://doi.org/10.1016/S0167-2991(96)80218-7.

Köseoḡlu, R.Ö., Phillips, C.R., 1987. Kinetics of non-catalytic hydrocracking of Athabasca bitumen. Fuel 66 (6), 741–748. https://doi.org/10.1016/0016-2361(87)90117-7.

Kohli, K., Prajapati, R., Maity, S.K., et al., 2019. Deactivation of a hydrotreating catalyst during hydroprocessing of synthetic crude by metal bearing compounds. Fuel 2019 (MAY 1), 579–589. https://doi.org/10.1016/j.fuel.2019.01.153.

Li, G.C., Liu, Y.Q., Tang, Z., et al., 2012. Effects of rehydration of alumina on its structural properties, surface acidity, and HDN activity of quinoline - ScienceDirect. Appl. Catal., A 437–438 (1), 79–89. https://doi.org/10.1016/j.apcata.2012.06.017.

Lu, M., Wang, A., Li, X., et al., 2007. Hydrodenitrogenation of quinoline catalyzed by MCM-41-supported nickel phosphides. Energy Fuel. 21 (2), 554–560. https://doi.org/10.1021/ef060467g.

Luan, Y.Z., Zhang, Q.M., He, D.M., et al., 2009. Hydrodenitrogenation of quinoline and its intermediates over sulfided NiW/γ-Al2O3 in the absence and presence of H2S. Asia Pac. J. Chem. Eng. https://doi.org/10.1002/apj.322.

Martens, G.G., Thybaut, J.W., Marin, G.B., 2001. Single-event rate parameters for the hydrocracking of cycloalkanes on Pt/US-Y zeolites. Ind. Eng. Chem. Res. 40 (8), 1832–1844. https://doi.org/10.1021/ie000799n.

Oh, Y., Shin, J., Noh, H., et al., 2019. Selective hydrotreating and hydrocracking of FCC light cycle oil into high-value light aromatic hydrocarbons. Appl. Catal., A 577, 86–98. https://doi.org/10.1016/j.apcata.2019.03.004.

Prada Silvy, R., Gaigneaux, E., Martens, J., et al., 2019. Scale-up of a NiMoP/γ-Al2O3 catalyst for the hydrotreating and mild hydrocracking of heavy gasoil. Oil Gas Sci. Technol. 74. https://doi.org/10.2516/ogst/2018094.

Prins, R., Jian, M., Flechsenhar, M., 1997. Mechanism and kinetics of hydrodenitrogenation. Polyhedron 16 (18), 3235–3246. https://doi.org/10.1016/S0277-5387(97)00111-3.

Scherzer Jg, A.J., 1996. Hydrocracking Science and Technology. Crc Press. https://doi.org/10.1016/S0255-2701(97)00020-2.

Speight, J.G., 2020. Hydrocracking - ScienceDirect. In: The Refinery of the Future, second ed., pp. 303–342.

Sun, M., Nelson, A.E., Adjaye, J., 2004. Correlating the electronic properties and HDN reactivities of organonitrogen compounds: an ab initio DFT study. J. Mol. Catal. Chem. 222 (1–2), 243–251. https://doi.org/10.1016/j.molcata.2004.08.015.

Sylvain, Cristol, Jean-Franois, et al., 2004. DBT derivatives adsorption over molybdenum sulfide catalysts: a theoretical study. J. Catal. 224 (1), 138–147. https://doi.org/10.1016/j.jcat.2004.02.008.

Tang, Z.J., Yang, Z.L., Wang, J.F., et al., 2017. Effects of impregnating solution properties on the performances of catalysts in hydrodenitrification. Petrochem. Technol. 46 (2), 177–182. https://doi.org/10.3969/j.issn.1000-8144.2017.02.006.

Tominaga, H., Nagai, M., 2010. Reaction mechanism for hydrodenitrogenation of carbazole on molybdenum nitride based on DFT study - ScienceDirect. Appl. Catal., A 389 (1), 195–204. https://doi.org/10.1016/j.apcata.2010.09.020.

Tung, N.T., Akira, S., Qian, E.W., 2017. Hydrodesulfurization, hydrodenitrogenation and hydrodearomatization over CoMo/SAPO-11-Al2O3 catalysts. J. Jpn. Petrol. Inst. 60 (6), 301–310.

Valles, V.A., Sa-Ngasaeng, Y., Martinez, M.L., et al., 2019. HDT of the model diesel feed over Ir-modified Zr-SBA-15 catalysts. Fuel 240 (MAR.15), 138–152. https://doi.org/10.1016/j.fuel.2018.11.148.

Yao, H., Wang, G., Zuo, C., et al., 2017. Deep hydrodenitrification of pyridine by solid catalyst coupling with ionic liquids under mild conditions. Green Chem. 19 (7), 1692–1700. https://doi.org/10.1039/C6GC03432B.

Zhang, X., Zhang, F., Yan, X., et al., 2007. Hydrocracking of heavy oil using zeolites Y/Al-SBA-15 composites as catalyst supports. J. Porous Mater. 15 (2), 145–150. https://doi.org/10.1007/s10934-007-9114-6.